Extreme Mechanics Letters 3 (2015) 105–112

Contents lists available at ScienceDirect

Extreme Mechanics Letters

journal homepage: www.elsevier.com/locate/eml

Push-to-pull tensile testing of ultra-strong nanoscale ceramic–polymer composites made by additive manufacturing☆

Jens Bauer [a,*], Almut Schroer [a], Ruth Schwaiger [a], Iwiza Tesari [a], Christian Lange [a], Lorenzo Valdevit [b], Oliver Kraft [a]

[a] Institute for Applied Materials (IAM), Karlsruhe Institute of Technology (KIT), Kaiserstr. 12, 76131 Karlsruhe, Germany

[b] Mechanical and Aerospace Engineering Department, University of California, Irvine (UCI), Irvine, CA 92697-3975, USA

GRAPHICAL ABSTRACT

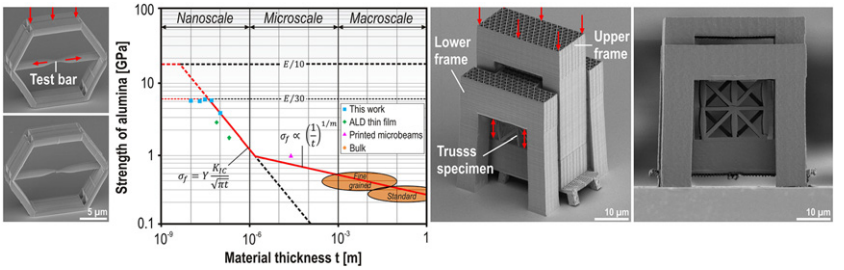

ARTICLE INFO

Article history:
Received 14 January 2015
Received in revised form 9 March 2015
Accepted 18 March 2015
Available online 24 March 2015

Keywords:
Size-effects
Theoretical strength
Alumina
Microarchitecture
3D-printing

ABSTRACT

The search for light yet strong materials recently benefited from novel high resolution 3D-printing technologies, which allow for fabricating lightweight porous materials with optimally designed micro-topologies. Architectural design improves mechanical properties significantly compared to stochastic porosity, as in foams. Miniaturization of the architectures offers to exploit material strengthening size-effects occurring at the nanoscale. However, these effects and their interaction with structural behavior are not yet well understood. We present tensile experiments of nanoscale alumina–polymer composite bars and cellular microarchitectures, applying 3D-printed push-to-pull mechanisms. The strength of alumina is found to strongly increase as the material thickness decreases. Below 50 nm thickness a plateau at about 5.5 GPa is reached, which is in the range of the theoretical strength. The characteristic low tensile strength of ceramics and its high variability seem not to hold at the nanoscale. Thus, when designed and fabricated appropriately, microarchitectures will facilitate carrying these size-effects beyond scales in future, allowing the use of ceramic materials far beyond what is possible to date.

☆ *Author Contribution*: J.B. and O.K designed research; J.B. and C.L. designed structures; J.B. and A.S. manufactured samples; J.B., A.S. and R.S. performed experiments; J.B. and I.T. performed finite-element simulations. J.B., O.K., L.V., R.S. and I.T. analyzed data; and J.B. wrote the paper .

* Corresponding author. Tel.: +49 721 60822129.
E-mail address: jens.bauer@kit.edu (J. Bauer).

http://dx.doi.org/10.1016/j.eml.2015.03.006
2352-4316/

1. Introduction

Various examples of microarchitected 3D-printed cellular materials (Fig. 1(a)), aiming to combine both outstanding mechanical properties and low density, have been published recently [1–4]. Regardless of the length-scale of structuring, optimally designed architectures exhibit superior mechanical properties compared to stochastic cellular materials, such as technical foams [5,6]. However, whether or not microarchitecture provides any significant advantage over macroscopic topologies, with respect to the strength-to-weight ratio, depends on the impact of size-dependent material strengthening effects [7–9]. These occur at the sub-micrometer to nanometer scale, and exploiting them at the cellular-material level requires a careful design of the microarchitecture.

Assuming a perfect crystal, the theoretical strength, σ_{th}, of brittle materials, such as ceramics, is considered to be of the order of 1/10 of their Young's modulus, E [7,11]. However, failure generally occurs at considerably lower stresses, since all solid materials contain a variety of imperfections, ranging from lattice defects on the atomic level to voids and cracks on the micro- and macro-scale.

At the nanometer scale, mechanical size-effects have been shown to strongly enhance the strength of brittle materials [7]. Certain biological ceramic-like materials, such as enamel [12], nacre [13] or bone [14], exploit that effects by hierarchical structuring, with only a few nanometers thin plate-like basic building units. At small dimensions, it can be assumed that the flaw size scales with the size of the component, which for the case of a thin plate, would correspond to its thickness. Thus, the strength increases with decreasing size, and has been predicted to reach theoretical strength at a critical thickness [7]. Arranging a large volume fraction of nano-sized platelets in a small amount of organic matrix nature produces tough and strong materials at the macroscale [7].

It remains a challenge to maintain extreme size-dependent strengthening, as observed in controlled nanomechanical experiments [9] across length scales, to make it accessible for macroscopic applications, such as achieving high toughness and reasonable strength, as nature does [7]. Microarchitected cellular materials provide a very promising avenue though. High-resolution 3D-printing [15–17] of polymeric truss- or shell-structures in conjunction with conformal coating techniques such as atomic layer deposition [18] (ALD) allows manufacturing of micro-architected ceramic [2,3] or ceramic–polymer composite [1] structures, with typical dimensions of individual structural elements in the micrometer range. The ceramic shells need to be fabricated sufficiently thin to gain enhanced strength but still thick enough to prevent structural instability, particularly in case of hollow structures [2,3], or poor reinforcement in case of a composite design [1]. For engineering ceramics, it is expected that the thickness of the shells need to be reduced to the order of 10 nm to fully exploit size-dependent strengthening. Whether due to exceeding the resolution limit of the printing method [3] or processing related design limitations [4], buckling or beam bending, both undesired when aiming for high strength, may occur.

3D direct laser writing [15] (3D-DLW) enables fabrication of truss structures with sub-micrometer resolution, and high freedom of design. Lightweight microarchitectures with densities well below 1 g/cm^3 were recently shown to reach strength-to-weight ratios comparable to those of bulk structural materials under uniaxial compression [1] (Fig. 1(b)). Of course, the overall volume of a sample which may be manufactured by 3D-DLW within a reasonable amount of time is currently below 1 mm^3. Nonetheless, as the scalability of high-resolution additive manufacturing increases rapidly, comprehensive characterization techniques that allow investigating size-dependent material strengthening, structural behavior and their interaction under different loading conditions are required.

Up to now, microarchitected cellular materials have only been characterized under compression, which may be related to experimental difficulties such as handling micro-size test samples. Without the need to grip samples, a push-to-pull construction transforms an applied compressive loading into a tensile load on a specimen. This test method was originally developed in the mid-20th century [19] for macroscopic samples, but has not been used extensively, due to high machining effort and material consumption [20]. More recently, it was adapted to microscale experiments [20], significantly reducing experimental effort and error related to sample mounting and load application.

In this paper, we present an approach to push-to-pull tensile characterization of nanoscale ceramic–polymer composite tensile bars (Fig. 2) as well as three-dimensional microarchitectures (Fig. 5). Using 3D-DLW, test specimens were integrally manufactured with a push-to-pull construction in one single production step from polymer (IP-Dip). Structures were conformally coated with alumina (Al_2O_3) layers of 10–100 nm thickness, resulting in a ceramic–polymer composite. We performed uniaxial *in* and *ex-situ* tensile tests for mechanical characterization.

Our results indicate that below a certain thickness in the range of 50 nm, the tested alumina layers can be considered to be insensitive to flaws, reaching strengths of the order of the theoretical limit. Once the architectural length-scale of a structure is small enough to apply such thin walls appropriately, size-effects in ALD alumina can fully be translated into cellular microarchitected materials of much larger scale, which are superior to macroscopically architected cellular materials. Outperforming most foam materials [10], we demonstrate micro-truss structures with a density of 0.2 g/cm^3 for 50 nm thick alumina coatings which exhibit tensile strengths of up to 7 MPa.

2. Experimental approach and results

2.1. Tensile bars

Push-to-pull tensile bar experiments were performed by designing hexagonal frames with integrated horizontal test struts (Fig. 2(a)). The structures consist of a polymer core, printed by 3D-DLW, and a conformal ALD alumina coating with 10–100 nm thickness. By using a nanoindentation system equipped with a flat punch tip, the frames

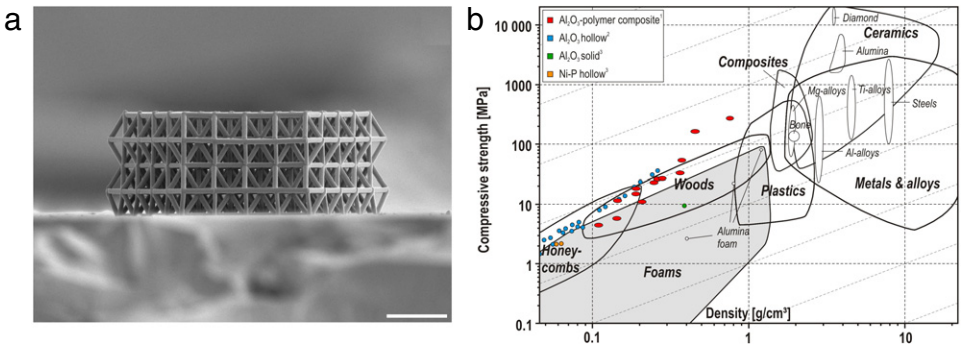

Fig. 1. 3D-printed lightweight microarchitected materials offer to combine specific structural design and size-dependent material strengthening effects which occur at the nanometer scale to achieve superior macroscale properties. (a) SEM image of a micro-truss from ceramic–polymer composite with strut diameters in the sub-micrometer regime (scale bar 10 μm). (b) Compressive strength–density chart [10]; reaching strength-to-weight ratios up to those of high-strength steels at a density well below 1 g/cm^3, microarchitected materials outperform natural and man made cellular materials (density calculated for ALD alumina with 2.9 g/cm^3, red and blue data points). (For interpretation of the references to color in this figure legend, the reader is referred to the web version of this article.)

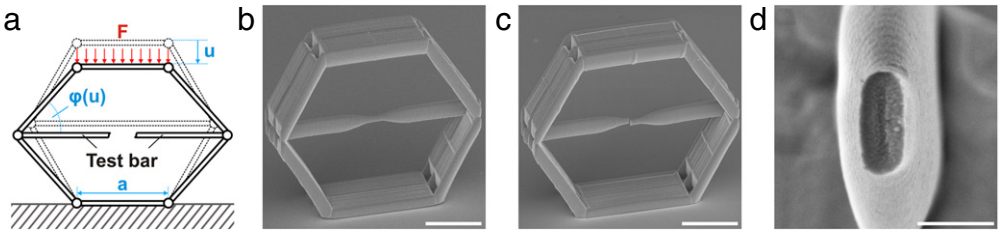

Fig. 2. Tensile characterization of nanoscale composite materials is facilitated by polymeric push-to-pull constructions, which are 3D-printed with integrated test bars and conformally coated with ceramic shells. Alumina coatings of 10–100 nm thickness were studied. (a) Loading the hexagon-shaped frame with the edge length, a, in compression puts the test bar under tension; load, F, and displacement, u, are recorded; the angle between the test bar and the frame is $\varphi(u)$. SEM images (b) before and (c–d) after testing with 10 nm thick coating are shown; test bars fracture in a brittle manner while the frame structure remains intact. (d) Fracture reveals the polymeric core and the ceramic shell on its surface. Scale bars are 5 μm (b–c) and 500 nm (d).

are loaded in compression at the top surface, putting the test bar under tension. Load, F, and displacement, u, of the indenter are recorded. Approximating the behavior of a hinged framework, the hexagon frame was designed much wider than the test bar, and slots at the joints as well as slight tapering of the frame struts towards them were applied to maximize joint flexibility (Fig. 2(b)). Test bars have a dog-bone shape, ensuring fracture at the center part with dimensions in the range of 500 nm in height and 200 nm in width (Fig. 2(d)). Without visible damage of the hexagonal frame, tensile bars fracture in a brittle manner (Fig. 2(c)–(d)).

For a quantitative analysis, tests with different geometries and conditions were performed (compare Supplementary Video 1–3, see Appendix A):

1. Empty hexagonal frames (without a test bar), with and without ALD coating.
2. Push-to-pull structures without coating, to determine the properties of the polymer.
3. Push-to-pull structures with ALD alumina with thickness from 10 to 100 nm, to measure the strength of the coatings.

Since the tensile bar and the frame joints act as elastic springs connected in parallel, load–displacement curves of empty frames can be subtracted from those of the actual push-to-pull tests, thus eliminating the effect of joint stiffness. The push-to-pull construction can be treated as an ideally pin-jointed framework subjected to the load difference, ΔF; from this, the load on the test bar, F_t, can be determined by

$$F_t = \frac{\Delta F}{\tan\varphi(u)} \tag{1}$$

where the angle between the test bar and the frame, $\varphi(u)$, is $\varphi(u) = \varphi_0 - a\sin(u/2a)$, with the initial angle $\varphi_0 = 60^\circ$ and the edge length of the hexagon frame $a = 10$ μm. The stress in the test bar is calculated by dividing F_t by the cross-sectional area of the center part of the bar (Supplementary Fig. 2, Supplementary Table 1, see Appendix A). Deformations are small, since tensile bars of coated structures fail when u roughly reaches 2% of the initial height of the frame. Therefore, the applied superposition is justified and has been verified by finite-element simulations (Supplementary Fig. 1, see Appendix A). Fig. 3(a) shows load–displacement curves for the push-to-pull mechanism, the empty frame and the extrapolated pin-jointed structure, for a purely polymeric sample. After the test bar has fractured, the curves for the push-to-pull and the empty frame structures obviously become identical.

Fig. 3(b) shows stress–displacement curves for the test bars for all tested coating thicknesses and for a polymer-only experiment. Except for the "elbow" at displacements below roughly 100 nm (generally related to small misalignment between the flat punch tip and the sample), all curves display linear elastic behavior.

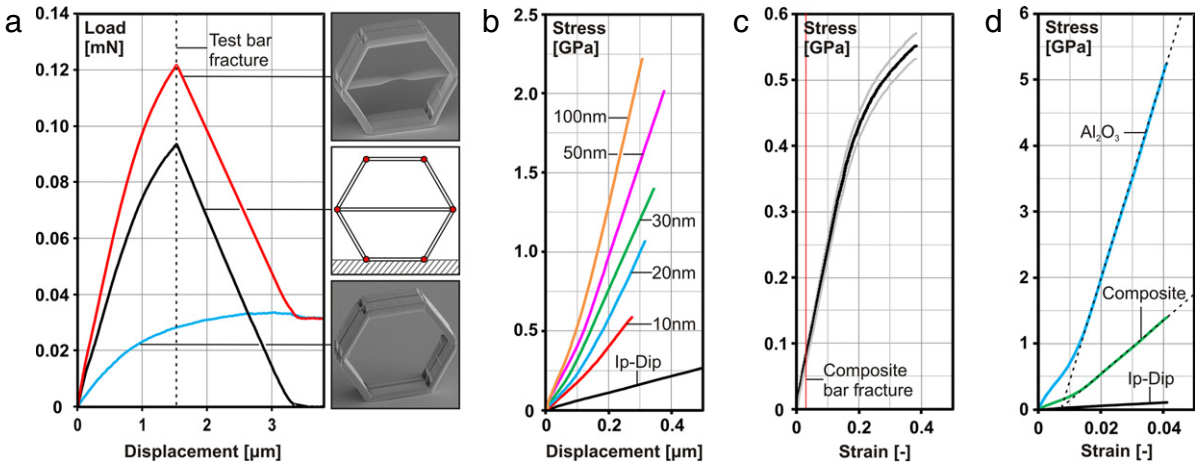

Fig. 3. Subtracting the test data of empty frames from that of actual push-to-pull tests with a test bar eliminates the influence of joint stiffness on the measured load. Thus, the systems can be treated as pin-jointed framework and the stress in the test bar determined analytically. (a) Load–displacement curves of uncoated push-to-pull construction with (red) and without (blue) a test bar, together with the corresponding subtraction, ΔF (black), which reflects the performance of a pin-jointed construction. (b) Dividing ΔF by the cross-sectional area of the center part of test bars provides stress–displacement curves of polymer and composite bars with different alumina coating thickness. (c) Average stress–strain curve of polymer-only test bars, the standard deviation of 5 tests is given in gray. (d) Measured stress–strain curves for a composite bar as well as the polymeric core and the calculated curve for the alumina coating (30 nm). (For interpretation of the references to color in this figure legend, the reader is referred to the web version of this article.)

Strain and Young's moduli of the composite, the polymer and the alumina shell were determined applying trigonometric correlations and the geometry of the test bar (Supplementary Fig. 2, Supplementary Table 1, see Appendix A). Stress–strain curves for the photo polymer IP-Dip, which serve as a reference for the measurements on ceramic–polymer composite bars, show elastic–plastic behavior with a yield strength of about 310 MPa and an ultimate tensile strength of approximately 550 MPa (Fig. 3(c)). The Young's modulus, E_p, for IP-Dip is found to be 2.34 ± 0.08 GPa, which agrees well with reported values for chemically similar photoresists such as SU-8 [21]. Assuming that only the center part of the dog bone shaped test bar is deformed plastically, the determined plastic strain to fracture of about 20% may be regarded as an upper limit, since some of the deformation is likely to occur in other parts of the structure.

The stress–strain relation for a representative composite bar (alumina thickness 30 nm) is shown in Fig. 3(d). The uniaxial stress in the composite test bar σ_c (red curve) is given by

$$\sigma_c = f_a\sigma_a + (1 - f_a)\sigma_p \tag{2}$$

where σ_a and σ_p are the stresses inside the alumina layer and the polymer core, respectively, and f_a is the area fraction of the coating layer. Eq. (2) can be transformed to

$$\sigma_a = \frac{\sigma_c - (1 - f_a)\sigma_p}{f_a} \tag{3}$$

giving the stress in the alumina layer (blue line) with $f_a = 25\%$. It is justified to assume linear elastic behavior of both materials for this analysis since fracture occurs at fairly small strains for which the polymer behaves elastically (Fig. 3(c)). The Young's modulus of alumina, E_a, is determined to be in the range of 165 ± 35 GPa, which is in agreement with literature values for ALD alumina [22].

The average values for the fracture strength of alumina as a function of the layer thickness are shown in Fig. 4. It is seen that the strength of ALD alumina is of the order of 3–5 GPa, which is 10 times higher than values for conventional bulk alumina, which are in the range of 250 MPa [10,23] to 600 MPa [10,24]. With decreasing coating thickness, the fracture strength of alumina strongly increases from 3.5 GPa at 100 nm to values of above 5 GPa for a thickness of 50 nm. Within the scatter of the data, the strength of the alumina layers between 10 and 50 nm is constant at about 5.2 GPa, which is close to $E/30$, when using a Young's modulus of 165 GPa for ALD alumina [22]. Remarkably, the scatter of the strength within test batches for each layer thickness was observed to be fairly low. Values for the Weibull modulus m of up to 69 have been obtained. It should be noted, however, that the number of tests was not sufficient to determine Weibull coefficients in a reliable manner. A summary of all experimental data is given in Supplementary Table 1 (see Appendix A).

2.2. Microarchitectures

For tensile testing of entire microarchitectures, we have developed a design, whereby a truss specimen is located between an upper and a lower frame construction (Fig. 5(a)–(b)). Pushing the upper frame downwards puts the test structure under tension (see Supplementary Video 4, see Appendix A). Prior to testing, auxiliary constructions from the fabrication have to be removed by focused ion beam milling. Processing and mechanical testing are similar to the previously described tensile bar experiments. To determine the effective applied tensile stress on the specimen, the measured load is directly divided by the nominal cross-sectional area of the test structure, not requiring further calculations. Clearly, manufacturing of such

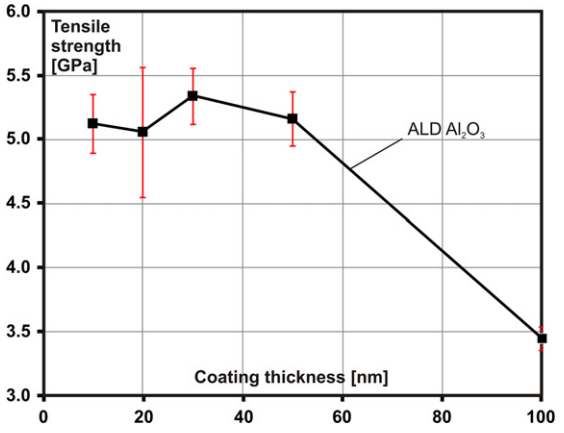

Fig. 4. The strength of alumina drastically increases at the nanoscale from 3.5 GPa at 100 nm thickness to values of up to 5.5 GPa for thicknesses below 50 nm. Error bars give the standard deviations of at least five tests per each coating thickness.

test samples is far more complex, than the single bar specimens discussed in Section 2.1, due to the large and massive frame construction, which requires a sophisticated laser-writing strategy. Truss structures made of cubic unit cells with diagonal bracings applied to each face have been examined. Their topology (referred to as "Design A") and mechanical behavior under compressive loads have been discussed in detail in Ref. [1].

Tensile test results for truss structures with 50 nm thick alumina coatings show a difference in the mechanical behavior compared to previously published compression tests [1] (Fig. 5(c)): Both strength and stiffness are lower in tension by a factor of 2. Nonetheless, the attained strength-to-weight ratio in tension, with stress values from 5.5 up to 7 MPa at a calculated density [1] of 0.2 g/cm^3, exceeds that of most technical foam materials [10]. All specimens failed by brittle fracture close to the truss joints (Fig. 5(b)).

3. Discussion

The proposed method of push-to-pull tensile testing for nanoscale ceramic composite bars has been shown to be an efficient way to measure the strength of ceramic films of 10–100 nm thickness. Mechanical characterization of thin films with thicknesses in that range is generally challenging, since sample fabrication and handling may be problematic; furthermore, macroscopic substrates, such as typically used in thin film nanoindentation, can significantly affect measurements [22]. The ability to rapidly manufacture large numbers of highly reproducible specimens by 3D-DLW, as well as the variety of possible coating materials and the simplicity of mechanical testing using a standard nanoindenter, qualifies the push-to-pull approach presented in this paper as a powerful method to characterize potential materials for microarchitecture and thin film materials in general. An accurate estimate of the Young's Modulus by push-to-pull testing is more challenging than to determine the strength. Experimental errors and uncertainty related to the geometrical dimensions multiply, especially when several materials are involved. This causes the fairly large error of ± 35 GPa in E_a which may be reduced with in situ strain measurements by digital image correlation in future work. The determination of σ_a at fracture, on the other hand, is much more accurate since E_p is smaller than E_a by a factor of $\sim$70 and therefore the possible stress range for σ_p remains narrow.

The observed tremendous increase in the strength of alumina shells with decreasing film thickness can be explained by the theory of size dependent strengthening described above [7]. For brittle materials, the fracture strength, σ_f, can be expressed as:

$$\sigma_f = Y \frac{K_{IC}}{\sqrt{\pi a}} \tag{4}$$

where K_{IC} is the fracture toughness of the material, a, is the length of the largest crack and Y, a non-dimensional parameter of order one, function of geometry and loading conditions [11]. Plasticity, which would reduce stress concentrations at crack tips, is not possible, leading to fracture at fairly low applied stress. As a result, the fracture strength from sample to sample is affected by scattering related to the statistical nature of size and orientation of cracks and other flaws [11]. Such weakest link failure can

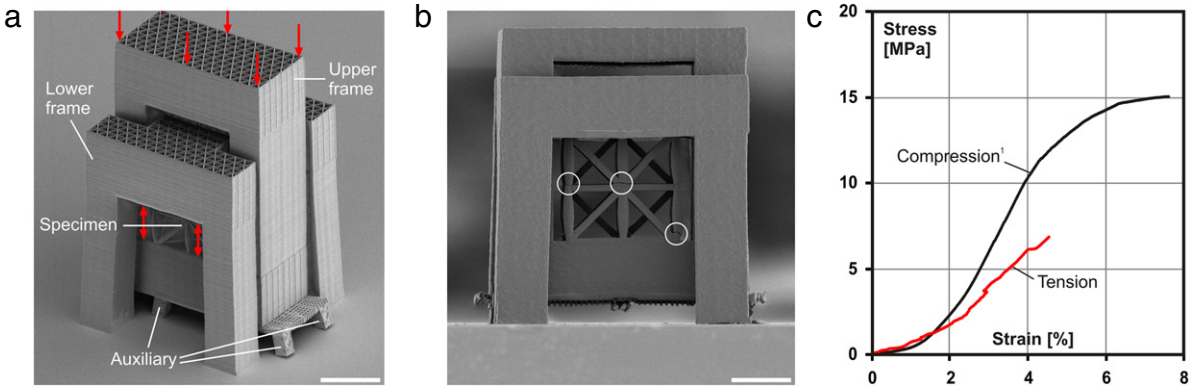

Fig. 5. Tensile testing of three-dimensional microarchitectures has been accomplished using the same principle and manufacturing route that was applied to one-dimensional tensile bars. SEM images of the structures (a) before and (b) after mechanical testing. The structures are located between an upper and a lower frame, and are loaded in tension by pushing the upper frame downwards. Auxiliary support structures from the production are removed by focused ion beam milling before testing. (b) Samples fail by brittle fracture close to the joints. (c) Strength and stiffness are roughly 50% lower in tension than in compression [1]. Scale bar is 10 μm for both (a) and (b).

be described by Weibull statistics where a measure for the variability in the strength is the Weibull modulus, m, with $m \to \infty$ meaning a perfectly deterministic strength and $m \to 0$ implying possible failure at any stress. While for ductile materials such as steel m is of the order of 100, for most engineering ceramics it is only in the range of 5–10 [11].

At the macro-scale, strength increases moderately when dimensions become smaller which can be described by Weibull statistics [25] by

$$\sigma_f \propto (1/t)^{1/m}. \tag{5}$$

Assuming a body made of volume elements containing a statistical distribution of flaws independent of the overall volume, with the largest crack causing failure, extreme flaws are more likely to occur when the number of volume elements and therefore the overall size of a component is larger [11]. The estimated high Weibull moduli of up to 69 in this work may be related to regular experimental scatter only, indicating that there is no characteristic weakest link failure at the nanoscale. However, to describe strong size-dependent strengthening observed here, Weibull statistics would require m to be very low. Therefore, in contrast to other studies [25], we do not consider that approach as appropriate.

At small dimensions, a can be assumed to scale with the size of the component, which for a shell is determined by its thickness, t. Following (4), the relation

$$\sigma_f \propto \frac{K_{IC}}{\sqrt{\pi t}} \tag{6}$$

may be derived, predicting strengthening of a shell structure when its thickness decreases [7]. According to (6), the fracture strength reaches the theoretical maximum σ_{th} at a certain critical thickness

$$t^* \propto \frac{1}{\pi}\left(\frac{K_{IC}}{\sigma_{th}}\right)^2 \tag{7}$$

below which materials are considered to be insensitive to flaws, implying the breakdown of classical fracture mechanics [7]. The highest possible notch stress at a crack tip at fracture is σ_{th}, thus brittle specimen containing a flaw fail at applied stresses lower than σ_{th} [11].

With $a = t$, $K_{IC} = 1.89$ MPa m$^{0.5}$ as the fracture toughness of ALD alumina [26] and $Y = 1$, the theoretical model is in good agreement with the experimental data of this work and of others' (Fig. 6). The results of this study may also support the claimed transition from size-dependent strengthening according to (6) to a regime where the strength remains in the range of σ_{th}, independent of the material thickness. However, with $E = 165$ GPa [22] the measured strength values are still considerably lower than $E/10$ when reaching a plateau below 50 nm thick layers, where the strength appears not to depend on the thickness anymore. On the other hand, with $\sigma_{th} = E/30$ a value originally derived by plastic failure, but also applied to ceramics as a lower bound [7,25], theory and experimental data match exceptionally well. The corresponding critical thickness t^* would be determined to be roughly 40 nm,

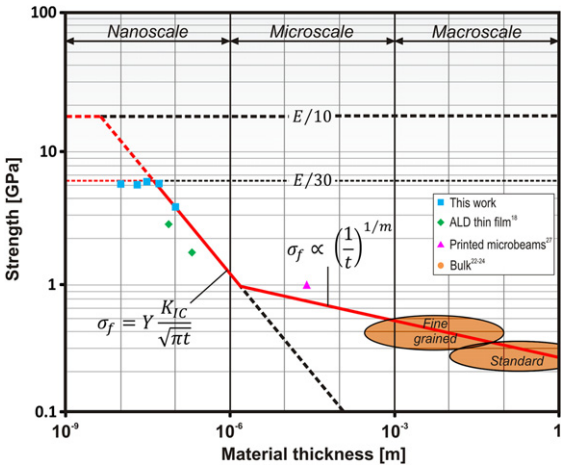

Fig. 6. Size dependent strengthening of alumina from the macro- to the nanoscale, theoretical model and experimental data [10,22–24,27]. The strength to thickness relation is described by different scaling laws.

which is in good agreement with the experimentally detected plateau below 50 nm. In the range below t^*, flaw-related failure may still be governing but there could be hardly any dependency of the flaw size on the shell thickness, causing the plateau. Possibly a lower limit flaw size range, related to the manufacturing process is reached. Therefore, (5) may be valid again below t^*, where values of m as high as 69 would cause a very mild dependency of strength and thickness. Atomic layer deposition can be assumed to cause fairly spherical pores rather than sharp cracks, which would imply a stress intensity factor reducing the attainable nominal stress by a factor in the range of two to three with respect to that of a perfect solid body.

Recent studies indicate that fully ceramic hollow lattices [2] obtained by polymer removal are structurally robust as well. On the other hand, it is known from constrained fracture of thin films [28,29] that the substrate may impede crack propagation, thus resulting in higher toughness than would be measured for a suspended film. Hence the presence of the polymer may play a beneficial role in supporting the alumina layers to achieve the large stresses discussed in this work. That effect needs to be quantified in further investigations.

The results of this work suggest that the two major shortcomings of macroscopic ceramics, namely, the low tensile strength and its high unpredictability, do not seem to be relevant at the nanometer scale. Microarchitecture may allow carrying these effects well beyond the nanoscale, opening the door for structural materials with unprecedented specific strength. Here we showed that maximum size-dependent strengthening of ALD alumina is reached in the range of 50 nm. When applying stiffer materials, that range is likely to shift to even lower values, since σ_{th} and therefore t^* scale with E. Thus, once the length scale of the architecture or its topology and shape do not allow layer thicknesses in the range of t^*, microarchitected materials may not have any significant structural advantage compared to similar materials with all dimensions at the macro-scale. And of course, the big effort of processing microarchitected materials needs to

be justified by substantial improvement. Such dramatic gains have been achieved in compressive loading of alumina–polymer composite structures, fabricated using 3D-DLW, which reached outstanding strength-to-weight ratios (see Fig. 1). The results of this study indicate that there is room for improvement, by scaling the architecture to even smaller dimensions.

Our novel push-to-pull tensile testing approach for three-dimensional micro-truss structures with several unit cells successfully pointed out the importance to characterize the tensile properties of entire microarchitectures as well. The high strength of alumina thin films obtained with one-dimensional tensile bars may not easily be exploited in complex three-dimensional structures. Although superior to most other cellular materials, the stiffness and strength under tension are significantly lower than under compression. With respect to stiffness, it is conceivable that this is related to an increased compliance of the frame construction in the push-to-pull structure itself. This error may easily be eliminated with in situ strain measurement by digital image correlation. Concerning the strength, failure under compression is initiated by local shear failure or buckling of struts [1]. In contrast, under tension, where crack formation is much more critical, notch stresses at the joints have a high impact, limiting the strength. Shape optimization at these joints may reduce stress concentrations to substantially increase the tensile strength of the micro-truss structures.

4. Methods

Experimental. We manufactured all presented structures by 3D-DLW (Photonic Professional; Nanoscribe GmbH) applying the photoresist IP-Dip (Nanoscribe GmbH). Polymeric structures were conformally coated with Al_2O_3 by ALD at 250 °C (Savannah 100; Cambridge NanoTech). A growth rate of 0.11 nm/cycle has been determined based on SEM measurements of micrometer thick coatings on a glass substrate. Polymer-only samples were vacuum-baked at 250 °C for 30 min prior to testing. For the mechanical characterization, we performed uniaxial compression tests at constant displacement rate (100 nm/s) using a nanoindenter (ex situ: Nanoindenter G200 XP; Agilent Technologies; in situ: InSEM, Nanomechanics Inc.) equipped with flat punch diamond tips of different diameters (tensile bar structures: 50 μm; truss structures: 100 μm). For each layer thickness at least five tests were performed.

Analysis. Assuming the hexagonal frame as ideally stiff, the elongation of the test bar, Δs, is given by $\Delta s = a\cos\varphi\,(u) - a/2$, and can be written as $\Delta s = \Delta s_1 + \Delta s_2 + \Delta s_3 = \varepsilon_1 l_1 + \varepsilon_2 l_2 + \varepsilon_3 l_3$, where Δs_i, ε_i, l_i are the corresponding elongations, strains and initial lengths of the different geometrical sections of the test bar (Supplementary Fig. 2, see Appendix A). With the maximum load-elongation slope $\Delta F_t^{\max}/\Delta s$ of polymer-only experiments, E_p can be determined by $E_p = \Delta F_t^{\max}/\Delta s\,(l_1/A_1 + l_2/A_2 + l_3/A_3)$. Within the linear elastic regime, the strain of the polymer is $\varepsilon_1 = F_t/(A_1 E_p)$; in order to include nonlinear effects such as plasticity, ε_1 may be written as $\varepsilon_1 = \left(\Delta s - F_t/E_p\,(l_2/A_2 + l_3/A_3)\right)/l_1$, assuming that those effects are concentrated in the center part of the test bar. For the composite, $1 = \Delta F_t^{\max}/\Delta s\,(l_1/(A_1E_1) + l_2/(A_2E_2) + l_3/(A_3E_3))$ is derived, with $E_i = f_{ai}E_a + (1 - f_{ai})E_p$; E_a can be determined recursively. For all tests, σ_p was in the range of 80 ± 20 MPa at the strain of composite bar fracture, and was determined with the relation $\sigma_c/E_1 = \sigma_p/E_p$.

Finite element simulations. Models of push-to-pull mechanisms with (real) and without (empty) a test bar as well as of an ideally pin-jointed structure (ideal) were compared (Supplementary Fig. 1, see Appendix A). Linear elastic material behavior has been assumed, with Young's moduli $E_a = 165$ GPa, $E_p = 2.34$ GPa and Poisson ratios of $\upsilon_a = 0.26$ and $\upsilon_p = 0.14$ for alumina and IP-Dip respectively. The tensile bar was modeled as a solid core (solid185) with a perfectly bonded coating layer (shell181). Polymeric core and ceramic coatings of hexagonal frames were modeled with shell elements (shell181), with the different material layers perfectly bonded. Translational and rotational degrees of freedom of coincident nodes at the end of the frame plates were coupled in the real and empty model. Only translational degrees of freedom were coupled in the ideal frame, to simulate hinged connections. In all models nodes aligned with the vertical mirror axis were clamped in horizontal direction, and edge nodes of the lower horizontal hexagonal plate were clamped in the vertical direction. A displacement was applied to the edge nodes of the top plate. Element sizes were $H_s/8$ in the hexagon frame and about $(h_i - b_i)/30$ in the test bar. Exploiting symmetry, models were reduced to 1/8 of the geometry to reduce computing effort. Simulations were carried out with ANSYS Academic Research 13.

Acknowledgments

Financial support by the Karlsruhe House of Young Scientists and the Robert Bosch Foundation is gratefully acknowledged.

Appendix A. Supplementary data

Supplementary material related to this article can be found online at http://dx.doi.org/10.1016/j.eml.2015.03.006.

References

[1] J. Bauer, S. Hengsbach, I. Tesari, R. Schwaiger, O. Kraft, High-strength cellular ceramic composites with 3D microarchitecture, Proc. Natl. Acad. Sci. USA 111 (2014) 2453–2458.
[2] L.R. Meza, S. Das, J.R. Greer, Strong, lightweight, and recoverable three-dimensional ceramic nanolattices, Science 345 (2014) 1322–1326.
[3] X. Zheng, et al., Ultralight, ultrastiff mechanical metamaterials, Science 344 (2014) 1373–1377.
[4] T.A. Schaedler, et al., Ultralight metallic microlattices, Science 334 (2011) 962–965.
[5] N.A. Fleck, V.S. Deshpande, M.F. Ashby, Micro-architectured materials: past, present and future, Proc. R. Soc. A Math. Phys. Eng. Sci. 466 (2010) 2495–2516.
[6] V.S. Deshpande, M.F. Ashby, N.A. Fleck, Foam topology: bending versus stretching dominated architectures, Acta Mater. 49 (2001) 1035–1040.
[7] H. Gao, B. Ji, I.L. Jaeger, E. Arzt, P. Fratzl, Materials become insensitive to flaws at nanoscale: lesson from nature, Proc. Natl. Acad. Sci. USA 100 (2003) 5597–5600.

[8] O. Kraft, P.A. Gruber, R. Mönig, D. Weygand, Plasticity in confined dimensions, Annu. Rev. Mater. Sci. 40 (2010) 293–317.
[9] T. Zhu, J. Li, Ultra-strength materials, Prog. Mater. Sci. 55 (2010) 710–757.
[10] CES EduPack. 2014. at: www.grantadesign.com.
[11] M.A. Meyers, K.K. Chawla, Mechanical Behavior of Materials, Cambridge University Press, 2009, pp. 404–523.
[12] E.D. Yilmaz, S. Bechtle, H. Özcoban, A. Schreyer, G.A. Schneider, Fracture behavior of hydroxyapatite nanofibers in dental enamel under micropillar compression, Scr. Mater. 68 (2013) 404–407.
[13] M.A. Meyers, A.Y.-M. Lin, P.-Y. Chen, J. Muyco, Mechanical strength of abalone nacre: role of the soft organic layer, J. Mech. Behav. Biomed. Mater. 1 (2008) 76–85.
[14] S. Weiner, H.D. Wagner, THE MATERIAL BONE: structure-mechanical function relations, Annu. Rev. Mater. Sci. 28 (1998) 271–298.
[15] G. Von Freymann, et al., Three-dimensional nanostructures for photonics, Adv. Funct. Mater. 20 (2010) 1038–1052.
[16] X. Zheng, et al., Design and optimization of a light-emitting diode projection micro-stereolithography three-dimensional manufacturing system, Rev. Sci. Instrum. 83 (2012) 125001.
[17] A.J. Jacobsen, W. Barvosa-Carter, S. Nutt, Micro-scale truss structures formed from self-propagating photopolymer waveguides, Adv. Mater. 19 (2007) 3892–3896.
[18] S.M. George, Atomic layer deposition?: An overview, Chem. Rev. 110 (2010) 111–131.
[19] A.J. Durelli, S. Morse, V. Parks, The theta specimen for determining tensile strength of brittle materials, Mater. Res. Stand. 2 (1962) 114–117.
[20] G.D. Quinn, et al., A novel test method for measuring mechanical properties at the small-scale: the theta specimen, Ceram. Eng. Sci. Proc. 26 (2005) 117.
[21] M. Hopcroft, et al., Micromechanical testing of SU-8 cantilevers, Fatigue Fract. Eng. Mater. Struct. 28 (2005) 735–742.
[22] M. Berdova, et al., Mechanical assessment of suspended ALD thin films by bulge and shaft-loading techniques, Acta Mater. 66 (2014) 370–377.
[23] D.W. Richerson, Modern Ceramic Engineering: Properties, Processing, and Use in Design, CRC Press Taylor & Francis Group, 2006, pp. 211–241.
[24] T. Fett, E. Ernst, D. Munz, D. Badenheim, R. Oberacker, Weibull analysis of ceramics under high stress gradients, J. Eur. Ceram. Soc. 23 (2003) 2031–2037.
[25] D. Jang, L.R. Meza, F. Greer, J.R. Greer, Fabrication and deformation of three-dimensional hollow ceramic nanostructures, Nature Mater. 12 (2013) 893–898.
[26] D.C. Miller, et al., The mechanical robustness of atomic-layer- and molecular-layer-deposited coatings on polymer substrates, J. Appl. Phys. 105 (2009) 093527.
[27] N.R. Philips, B.G. Compton, M.R. Begley, High strength alumina micro-beams fabricated by inkjet printing, J. Am. Ceram. Soc. 95 (2012) 3016–3018.
[28] J.W. Hutchinson, Z. Suo, Mixed mode cracking in layerd materials, Adv. Appl. Mech. 29 (1991) 63–191.
[29] R.F. Cook, Z. Suo, Mechanisms active during fracture under constraint, MRS Bull. 27 (2002) 45–51.